Supplementary Information

Catalyst Support for Direct-Ammonia Solid-Oxide Fuel Cell Anodes based on Lanthanum Titanium Oxynitride

Saurav Sorcar[1#], Hodaya Zinowitz[1#], Eswaravara Prasadarao Komarala[1], Nomi Moshe[1], Ira Agranovich[1], Brian A. Rosen[1]*

[1]Department of Materials Science and Engineering, Tel Aviv University, Ramat Aviv 6997801, Israel

[#]Authors with equal contribution
*Corresponding author: barosen@post.tau.ac.il

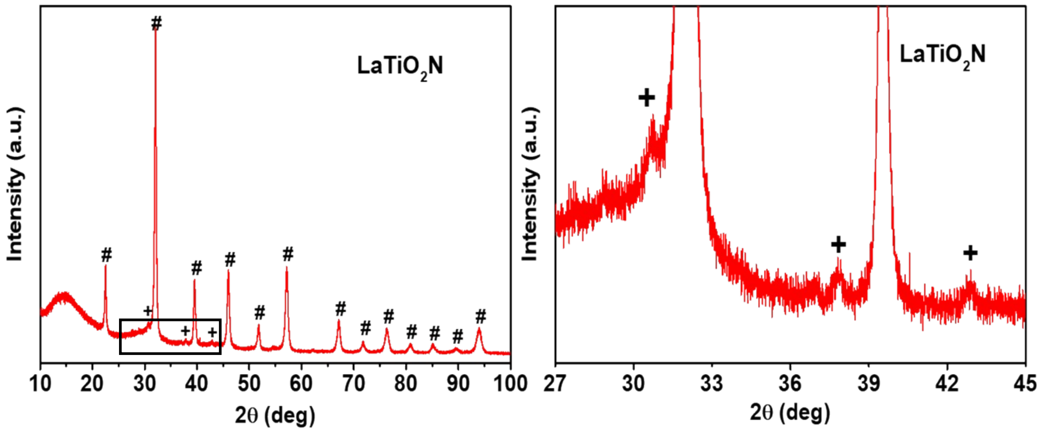

Figure. S1 XRD result of $LaTiO_2N$ and its corresponding zoomed in data from 2Θ values 27° to 46°. (# $LaTiNO_2$ PDF: 04-014-5881), (+Ti_5O_9 PDF: 04-005-4465)

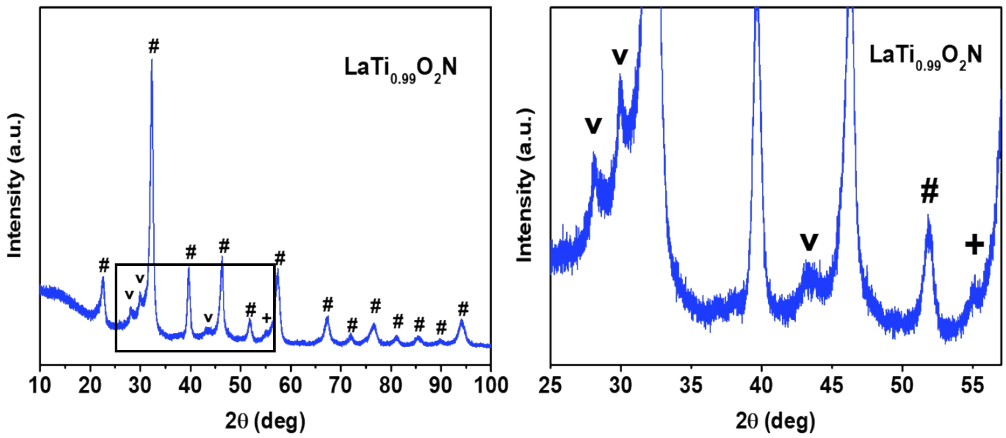

Figure. S2 XRD result of $LaTi_{0.99}O_2N$ and its corresponding zoomed in data from 2Θ values 25° to 57°. (# $LaTiNO_2$ PDF: 04-014-5881), (∨ $La_2Ti_2O_7$ PDF: 00-015-0334), (+ Ti_5O_9 PDF: 04-005-4465)

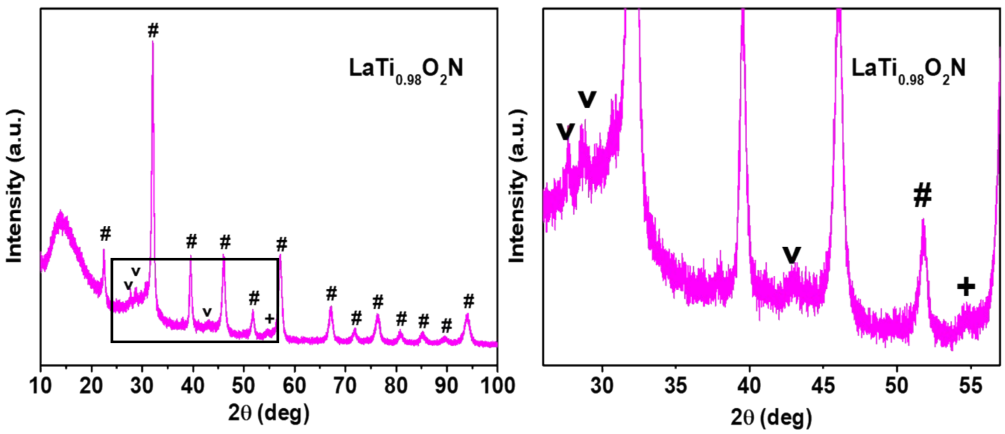

Figure. S3 XRD result of $LaTi_{0.98}O_2N$ and its corresponding zoomed in data from 2ϴ values 26° to 57°. (# $LaTiNO_2$ PDF: 04-014-5881), (∨ $La_2Ti_2O_7$ PDF: 00-015-0334), (+ Ti_5O_9 PDF: 04-005-4465)

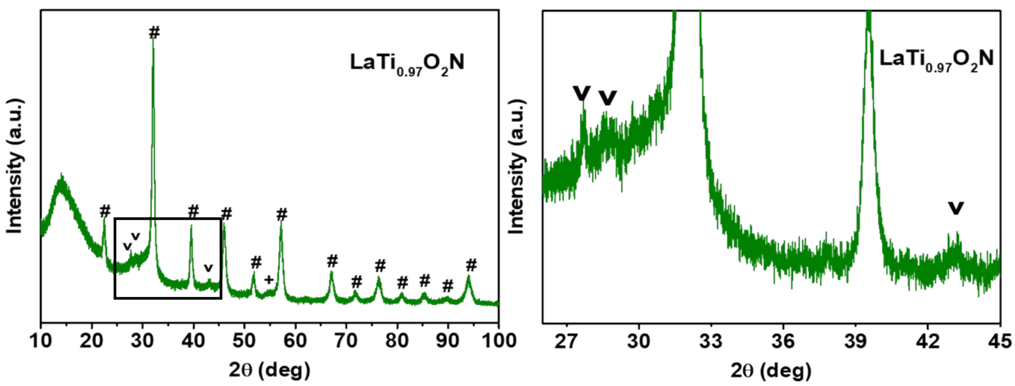

Figure. S4 XRD result of $LaTi_{0.97}O_2N$ and its corresponding zoomed in data from 2ϴ values 26° to 45°. (# $LaTiNO_2$ PDF: 04-014-5881), (∨ $La_2Ti_2O_7$ PDF: 00-015-0334), (+ Ti_5O_9 PDF: 04-005-4465)

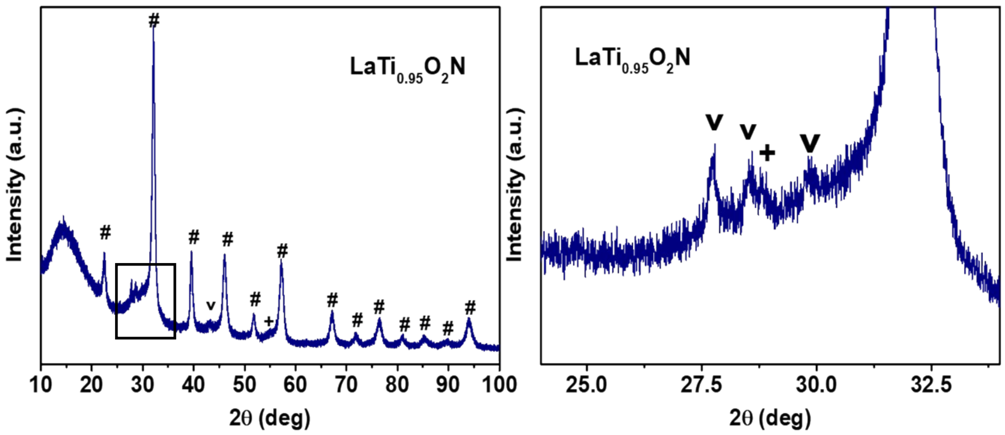

Figure. S5 XRD result of $LaTi_{0.95}O_2N$ and its corresponding zoomed in data from 2Θ values 24° to 34°. (# $LaTiNO_2$ PDF: 04-014-5881), (+ Ti_5O_9 PDF: 04-005-4465), (∨ $La_2Ti_2O_7$ PDF: 00-015-0334)

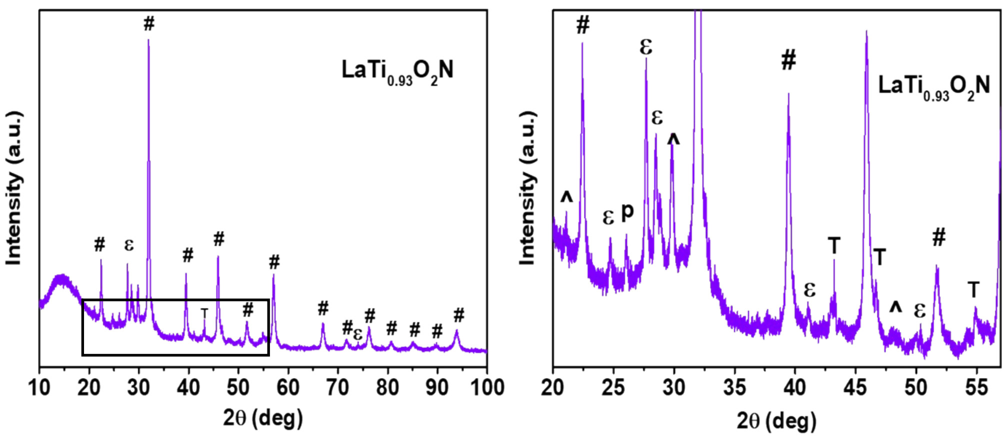

Figure. S6 XRD result of $LaTi_{0.93}O_2N$ and its corresponding zoomed in data from 2Θ values 20° to 57°. (# $LaTiNO_2$ PDF: 04-014-5881), (**T** Ti_6O_{11} PDF: 00-050-0788), (^ $La_2Ti_2O_7$ PDF: 04-006-7220), (**ε** La_2TiO_5 PDF: 04-011-9299), (**p** $La_{1.6}Ti_{0.4}O_3$ PDF: 04-001-6803)

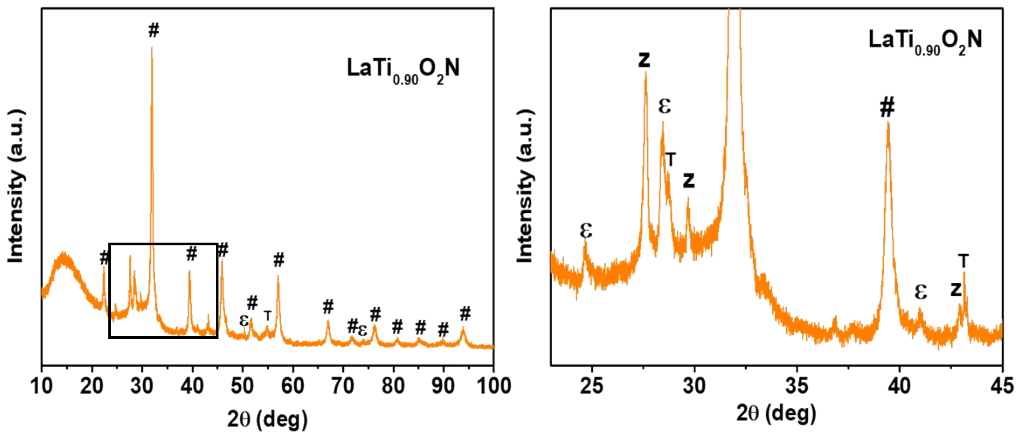

Figure. S7 XRD result of $LaTi_{0.90}O_2N$ and its corresponding zoomed in data from 2Θ values 23° to 45°. (# $LaTiNO_2$ PDF: 04-014-5881), (**T** Ti_6O_{11} PDF: 00-050-0788), (**ε** La_2TiO_5 PDF: 04-011-9299), (**Z** $La_2Ti_2O_7$ PDF: 00-017-0451)

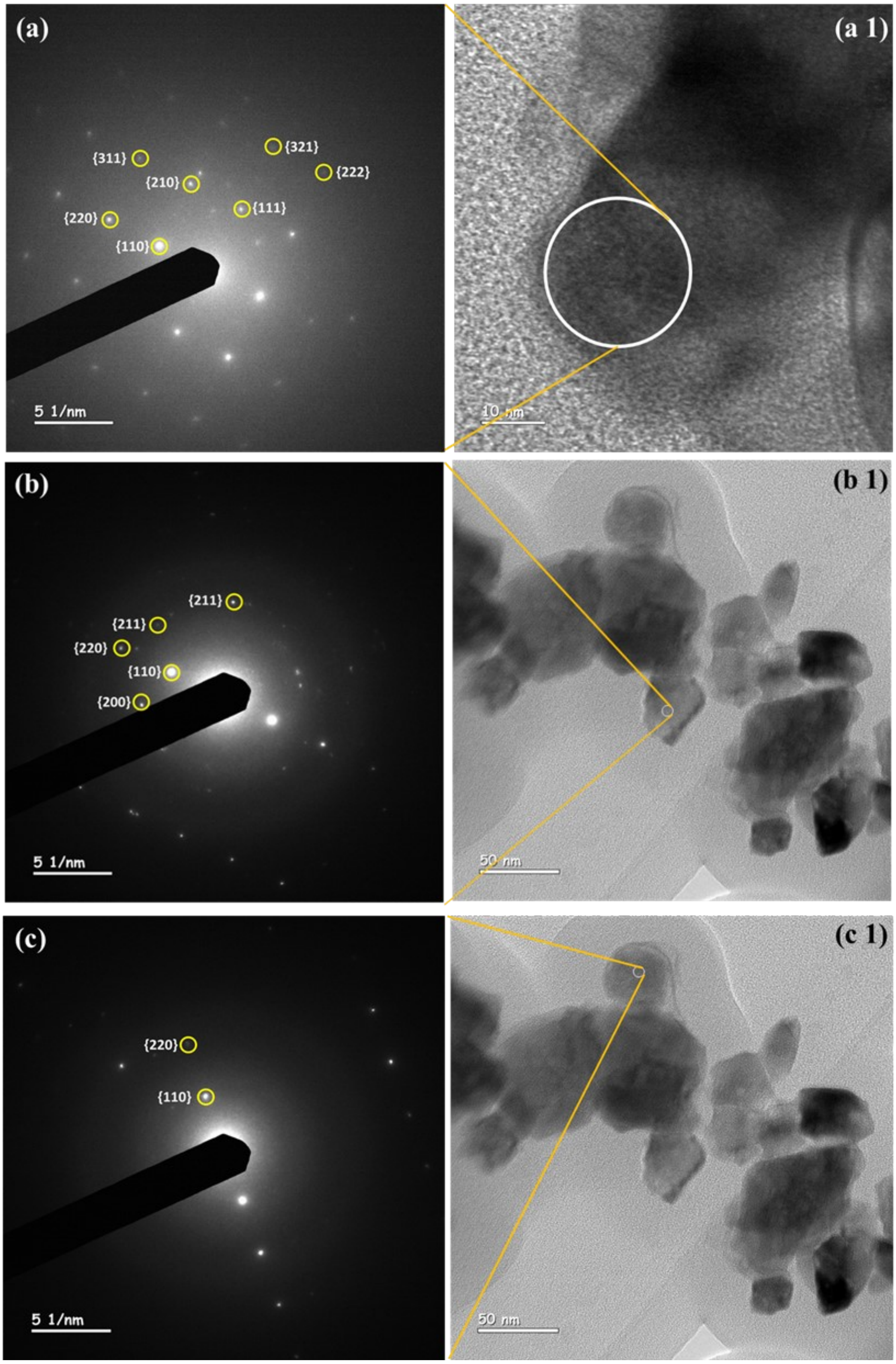

Figure S8. (a), (b), and (c) SAED results of the circled region (a1), (b1), and (c1), respectively, for the sample 5%Cu-LTON. The unlabeled peaks without a symmetrical point on the other side of the beam are expected to be contaminating phase (identified by XRD) out of zone axis.

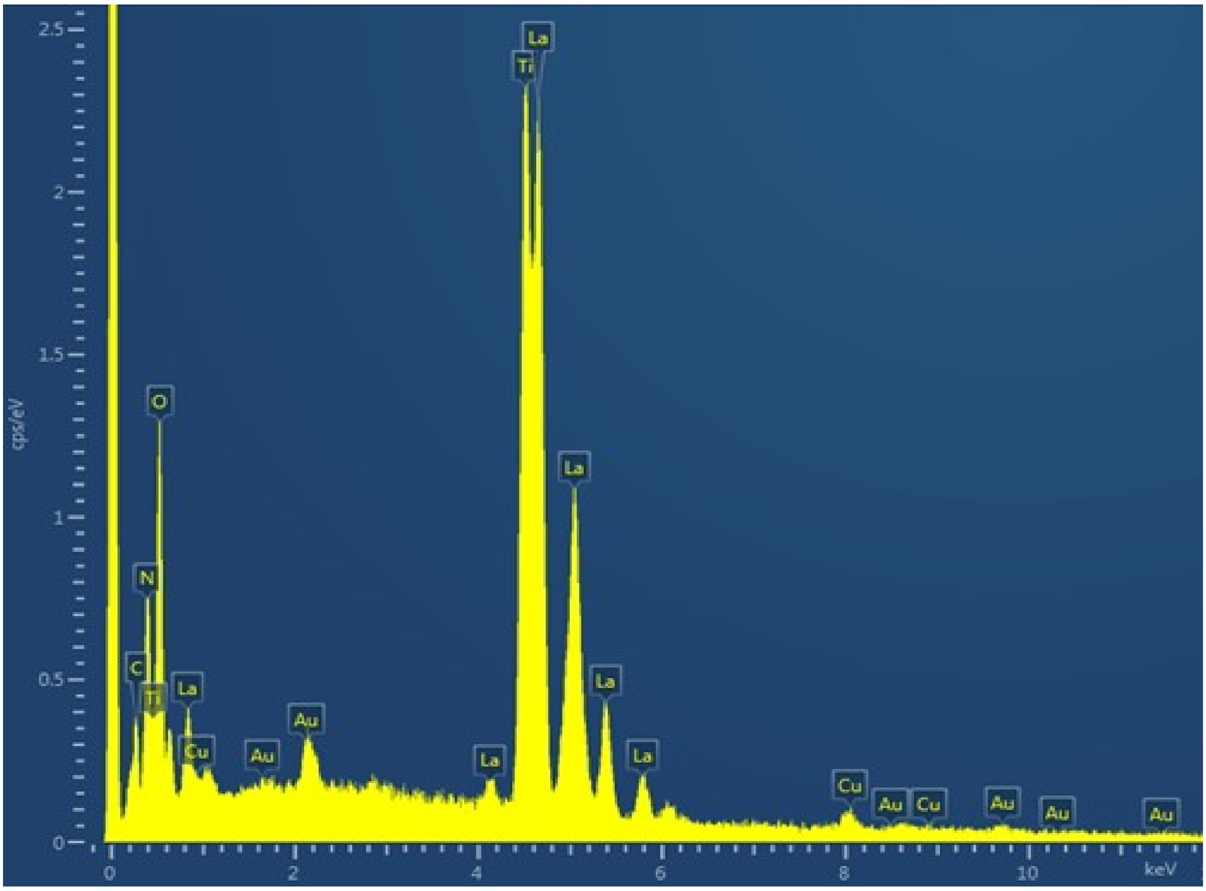

Figure S9. SEM-EDS analysis of 5%Cu-LTON.

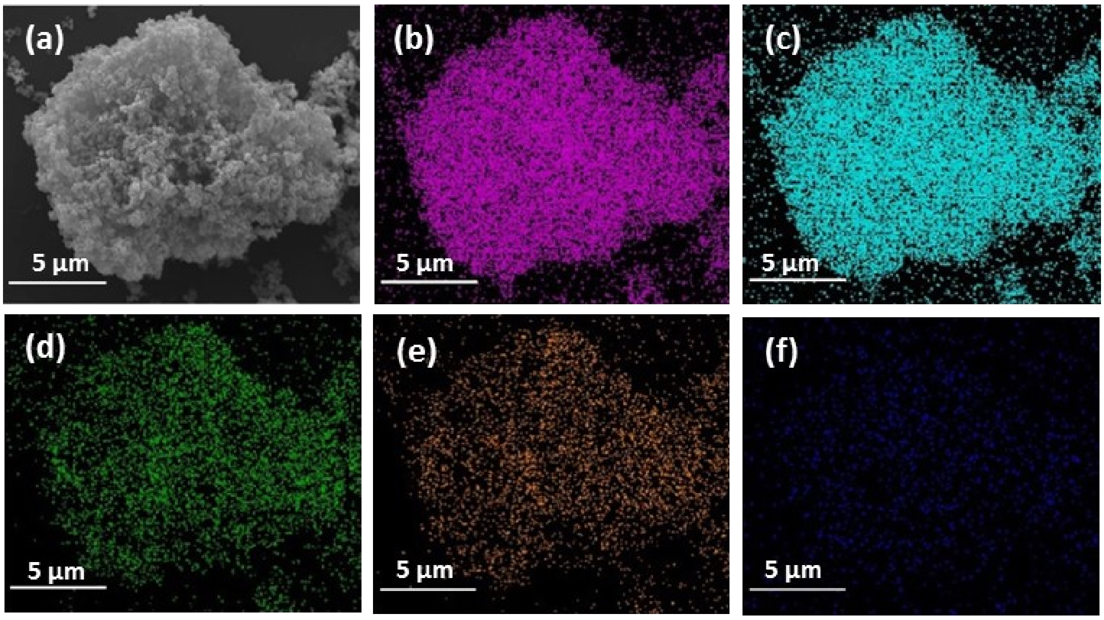

Figure S10. (a) SEM backscatter image of an agglomerated Cu-LTON support and EDS elemental mapping of Cu-LTON showing the distribution of (b) La, (c) Ti, (d) O, (e) N, and (f) Cu.

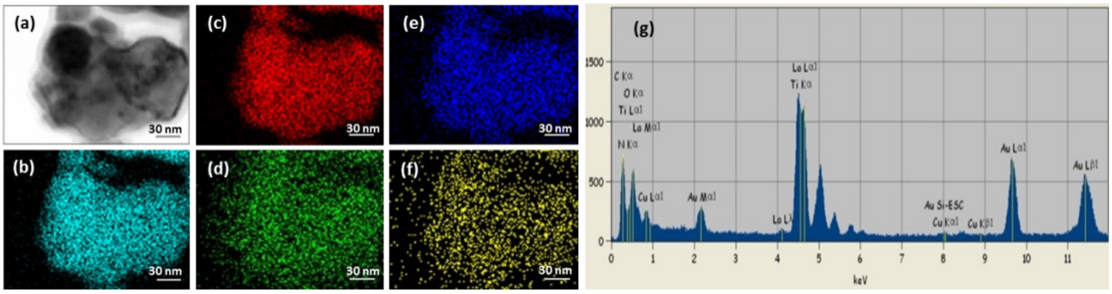

Figure S11. (a) Bright-field TEM image of 5%Cu-LTON and its corresponding, EDX-STEM mapping showing the distribution of (b) La, (c) Ti, (d) N, (e) O, (f) Cu, and (g) TEM-EDS image.

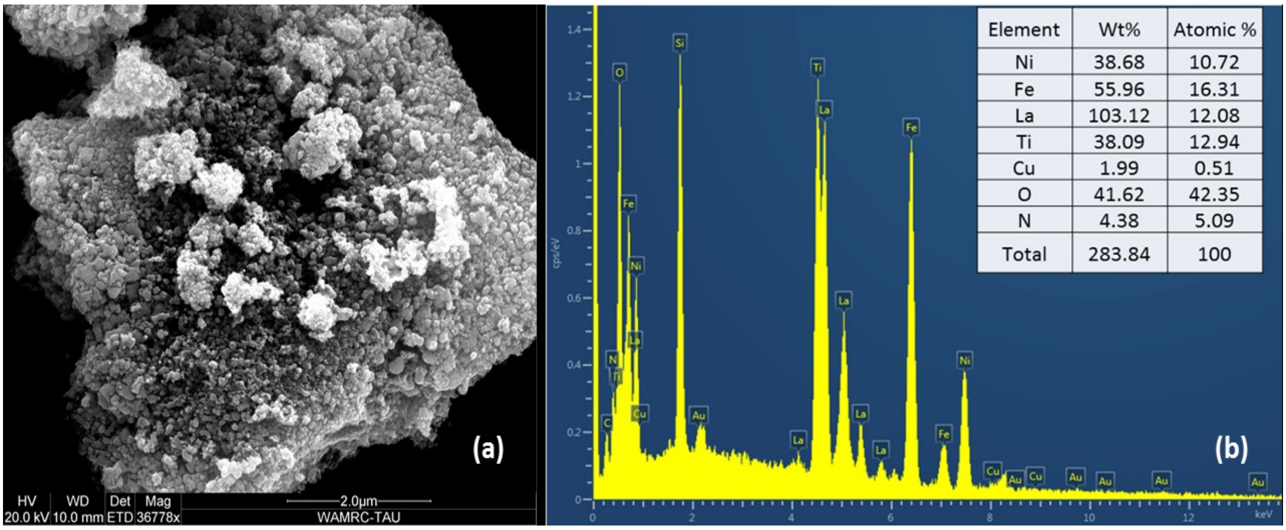

Figure S12. (a) SEM image of $Ni_{15}Fe_{21}$/5%Cu-LTON and its (b) EDS analysis.

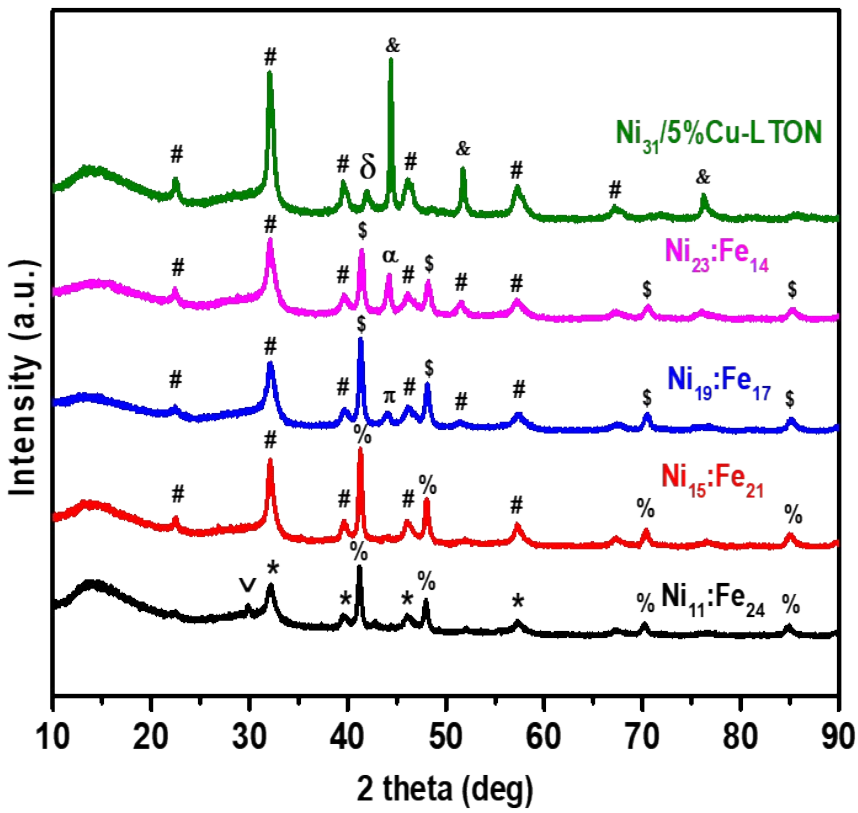

Figure S13. Powder XRD patterns of Ni_YFe_Z/5%Cu-LTON samples. (# $LaTiNO_2$ 04-014-5881), (˅ $La_2Ti_2O_7$ 00-028-0517), (* $LaTiO_2N$ 00-048-1230), (% Fe_3NiN 00-009-0318), ($ Fe_2Ni_2N 00-050-1350), (π $Fe_{0.4}Ni_{0.6}$ 04-004-8867), (α $Fe_{0.15}Ni_{0.85}$ 04-024-7186), (& Ni 04-010-6148), (δ La_5Ni_{19} 04-017-4192).

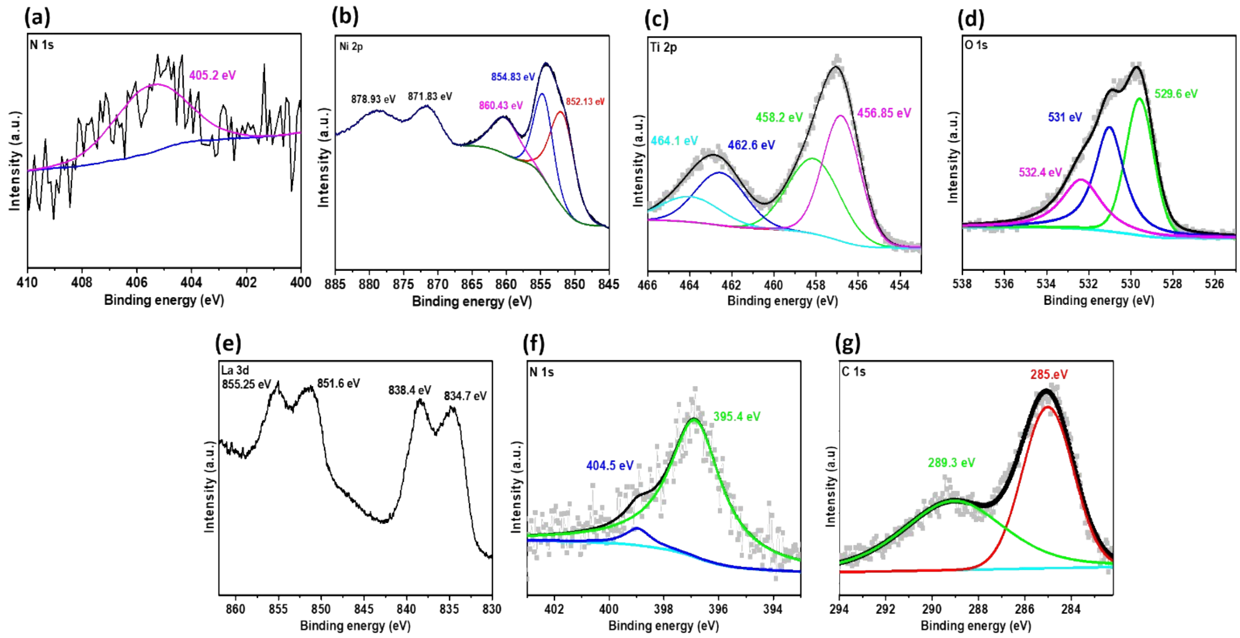

Figure S14. HR- XPS results (a) N 1s, (b) Ni 2p of Ni_{31}/5%Cu-LTON treated under 5% H_2 and (c) Ti 2p, (d) O 1s, (e) La 3d, (f) N 1s, and (g) C 1s for the 5%Cu-LTON catalyst.

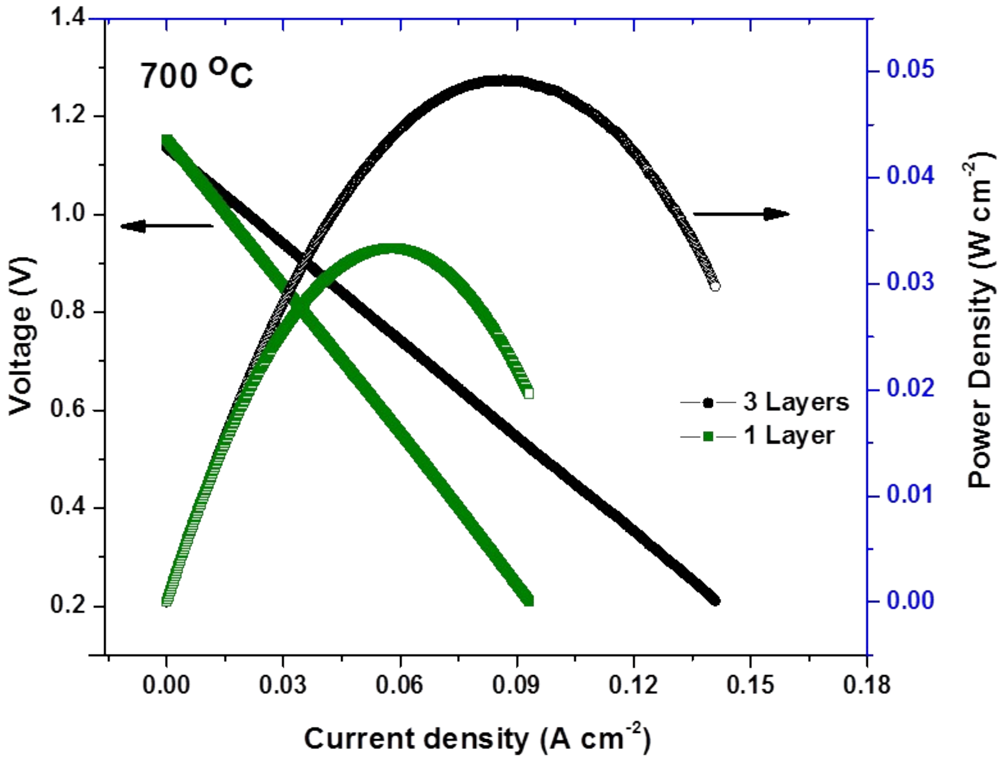

Figure S15. Single layer vs three layer I-V curves of $Ni_{15}Fe_{14}$/5% Cu-LTON anode SOFC.

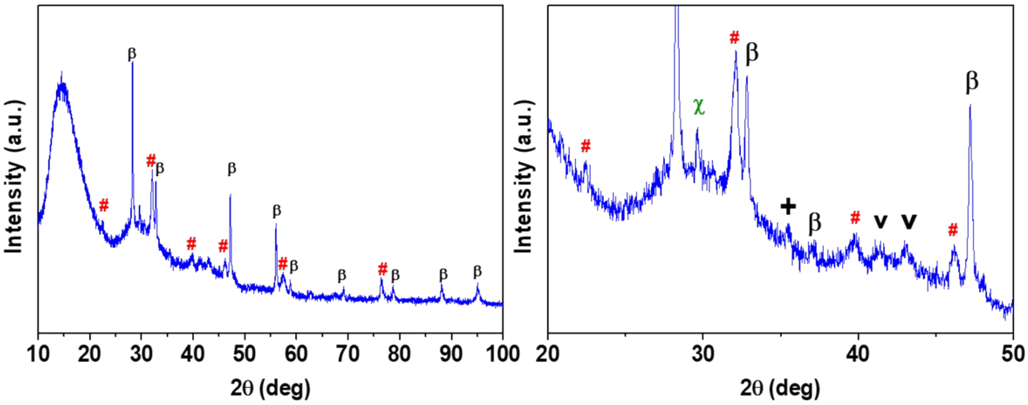

Figure S16. XRD results of used DA-SOFC cell Ni_{15}:Fe_{21} / 5%Cu-LTON.

(* $LaTiO_2N$ PDF: 00-048-1230), (β $Ce_{1.5}Gd_{0.5}O_{3.75}$ PDF: 04-020-7979), (χ $Y_4Zr_3O_{12}$ PDF: 04-002-0211), (∨ $La_2Ti_2O_7$ PDF: 00-015-0334), (+ Ti_5O_9 PDF: 04-005-4465)

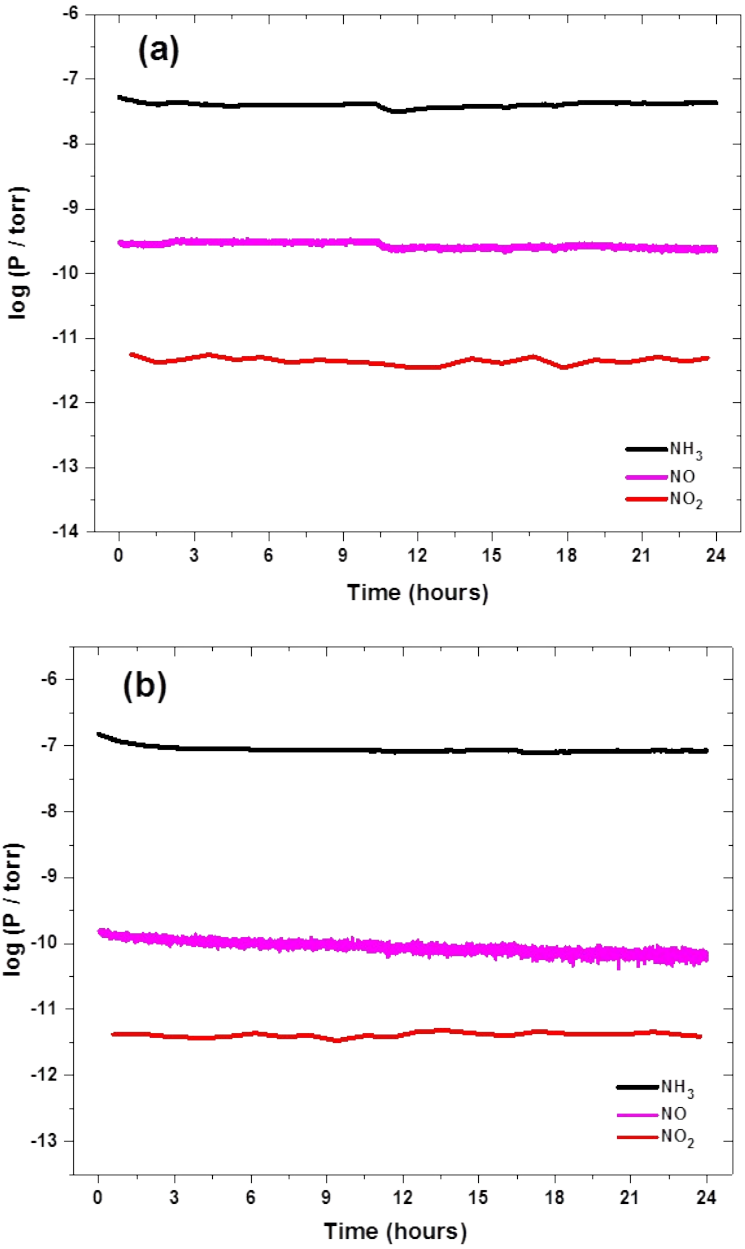

Figure S17. Partial pressure curves of NH_3 and NO_x gases of (a) $Ni_{15}Fe_{21}$/5%Cu-LTON cell and (b) $Ni_{19}Fe_{17}$/5%Cu-LTON cell are presented. The curves show the partial pressure of the gases as a function of time during 24 hours at 750^0C temperature. The total pressure in the vacuum system was $6.3*10^{-6}$torr.

Table S1. SEM-EDS elemental analysis results of $LaTi_{0.95}O_2N$.

	La	Ti	O	N	Stoichiometry
Sample 1	17.32	17.88	53.8	10.99	$La_{1.00}Ti_{1.03}O_{3.10}N_{0.63}$
Sample 2	15.39	16.12	55.96	12.53	$La_{1.00}Ti_{1.04}O_{3.63}N_{0.81}$
Sample 3	18.8	17.14	52.71	11.34	$La_{1.00}Ti_{0.91}O_{2.8}N_{0.60}$
Sample 4	14.52	15.09	58.57	11.82	$La_{1.00}Ti_{1.03}O_4N_{0.81}$

Table S2. SEM-EDX elemental analysis results of 5%Cu/LTON

	Cu	**La**	**Ti**	**O**	**N**	**Stoichiometry**
Sample 1	0.96	15.2	16.75	51.3	15.78	$Cu_{0.06}$-$La_{1.00}Ti_{1.10}O_{3.37}N_{1.03}$
Sample 2	0.9	16.43	16.82	53.01	12.84	$Cu_{0.05}$-$La_{1.00}Ti_{1.02}O_{3.22}N_{0.78}$
Sample 3	1.75	19.45	22.7	42.63	13.48	$Cu_{0.09}$-$La_{1.00}Ti_{1.16}O_{2.19}N_{0.69}$
Sample 4	0.86	15.71	16.38	56.61	10.44	$Cu_{0.05}$-$La_{1.00}Ti_{1.04}O_{3.6}N_{0.66}$

Table S3: Peak powder densities of ammonia-fueled SOFCs having YSZ electrolyte.

Anode	**Cathode**	**Operating Temperature [^oC]**	**YSZ Electrolyte Thickness [µm]**	**Peak Power Density [$mWcm^{-2}$]**
Ba-Ni-YSZ	LSCF	750	10	275 [1]
NiO/YSZ	LSCF	750	10	195[2]
NiO/YSZ	LSM-YSZ	800	15	202 [3]
Ni-YSZ	LSF	700	4-6	325 [4]
Ni-YSZ	LSM-YSZ	750	30	299 [5]
Ni-YSZ	LSM-YSZ	700	--	38[6]
Ni:Fe/Cu-LTON+GDC (This study)	***LSCF-GDC***	***750***	***43***	***230***

Table S4. SEM-EDX elemental analysis results of used cell Ni_{15}:Fe_{21}/5%Cu-LTON.

	Cu	La	Ti	O	N	Ni	Fe	Gd	Ce	C
Site 1	0.17	3.86	3.86	65.12	0.46	3.59	4.45	0.52	5.49	12.48
Site 2	0.13	2.85	2.86	66.39	0.56	2.87	4.52	0.33	4.11	15.39
Site 3	0.12	2.98	2.97	68.71	0.3	3.63	6.09	0.39	4.82	9.98
Site 4	0.31	3.05	3.14	55.57	1.19	4.07	6.97	0.8	11.18	13.73
Site 5	0.04	3.3	3.35	64.23	0.48	3.34	5.2	0.69	6.36	13
Site 6	0.08	3.1	2.96	64.58	0.53	3.45	4.89	0.72	7.12	12.55

References:

[1] Y. Wang, J. Yang, J. Wang, W. Guan, B. Chi, L. Jia, J. Chen, H. Muroyama, T. Matsui, K. Eguchi, Low–Temperature Ammonia Decomposition Catalysts for Direct Ammonia Solid Oxide Fuel Cells, J. Electrochem. Soc. 167 (2020) 064501. https://doi.org/10.1149/1945-7111/ab7b5b.

[2] M. Zendrini, M. Testi, M. Trini, P. Daniele, J. Van Herle, L. Crema, Assessment of ammonia as energy carrier in the use with reversible solid oxide cells, Int. J. Hydrogen Energy. 46 (2021) 30112–30123. https://doi.org/10.1016/j.ijhydene.2021.06.139.

[3] L. ZHANG, Y. CONG, W. YANG, L. LIN, A Direct Ammonia Tubular Solid Oxide Fuel Cell, Chinese J. Catal. 28 (2007) 749–751. https://doi.org/10.1016/S1872-2067(07)60062-X.

[4] J. Yang, A.F.S. Molouk, T. Okanishi, H. Muroyama, T. Matsui, K. Eguchi, A Stability Study of Ni/Yttria-Stabilized Zirconia Anode for Direct Ammonia Solid Oxide Fuel Cells, ACS Appl. Mater. Interfaces. 7 (2015) 28701–28707. https://doi.org/10.1021/acsami.5b11122.

[5] Q. Ma, J. Ma, S. Zhou, R. Yan, J. Gao, G. Meng, A high-performance ammonia-fueled SOFC based on a YSZ thin-film electrolyte, J. Power Sources. 164 (2007) 86–89. https://doi.org/10.1016/j.jpowsour.2006.09.093.

[6] A. Fuerte, R.X. Valenzuela, M.J. Escudero, L. Daza, Ammonia as efficient fuel for SOFC, J. Power Sources. 192 (2009) 170–174. https://doi.org/10.1016/j.jpowsour.2008.11.037.